

Numerical Simulations of Unsteady Low-Reynolds-Number Flows Over the APEX Airfoil

Mahidhar Tatineni* and Xiaolin Zhong†

University of California, Los Angeles, California 90095

Abstract

Laminar and transitional separation bubbles are an important feature of low-Reynolds-number flows over airfoils. The separation bubbles are unsteady and have a significant impact on the aerodynamic properties of the airfoils. In this paper unsteady low-Reynolds-number separated flows over the APEX airfoil are calculated using a Navier-Stokes solver. The numerical results show the presence of unsteady separation bubbles in the flowfield. An analysis of the numerical results shows that flowfield disturbances are amplified significantly in the separation bubble, leading to periodic vortex shedding. A linear stability analysis of the separated boundary layer is performed and the results show that the dominant wavenumber and frequency in the numerical simulations agree with the most unstable wavenumber and frequency from the linear stability analysis. The numerical results also show the growth and interaction of disturbance waves in the separation bubble. For transonic flows over the APEX airfoil, the calculations show that the presence of shocks causes significant changes in the separation location and consequently, the overall flowfield.

INTRODUCTION

The aerodynamic characteristics of airfoils in the low-Reynolds-number regime (ranging from $Re = 5 \times 10^4$ to 1×10^6) are required for a variety of applications ranging from turbine blades to sailplanes and high altitude unmanned aerial vehicles (UAV's).^[1,2] Hence, low-Reynolds-number flows over airfoils have been the subject of many experimental^[3-7] and computational^[8-11] studies. The current research is motivated by the APEX project at NASA Dryden Flight Research Center which will use a high altitude aircraft to collect aerodynamic data in the transonic low-Reynolds-number flow regime.^[2]

The flowfield in low-Reynolds-number flows over airfoils is strongly influenced by the presence of laminar-turbulent separation bubbles. Figure 1(a) shows a schematic of the structure of a separation bubble. The laminar flow separates due to the adverse pressure gra-

dient. The separated boundary layer is unsteady, and usually becomes unstable and rapidly undergoes transition. The turbulent flow reattaches, and the region between the separation point and the reattachment point is called the separation bubble. The separated region is usually highly unstable and characterized by significant growth of disturbance waves. This is shown in Fig. 1(b) which illustrates the transition process as the linear growth of disturbances corresponding to the instability of the separated flow, followed by nonlinear interaction of disturbances leading to turbulent flow.

The strong influence of the separation bubbles on the performance of airfoils in low-Reynolds-number flows has been shown in many experimental studies.^[3,4,7] The structure of the unsteady separation bubbles has been studied through experimental investigations of the growth of disturbance waves and the transition process. Leblanc, Blackwelder, and Liebeck^[5] measured the dominant frequencies in the velocity spectra in the separated region. They showed that the peak frequencies measured in the velocity spectra for the instability region match the most amplified wavenumber and frequency scaling calculated by linear stability theory. Dovgal, Kozlov, and Michalke^[6] also confirmed the linear growth of disturbances in the separated region. They also showed that the subsequent nonlinear interactions of the disturbance waves led to transition. An important observation was that the mean flow is changed by the presence of disturbance waves in the flowfield.

Drela and Giles^[8,12] used a viscous-inviscid approach to compute transonic low-Reynolds-number flows over airfoils. Their calculations show the strong influence of separation bubbles on the overall flowfield, and predicted the rapid degradation in the performance of the airfoils with decreasing Reynolds-numbers. Lin and Pauley^[11] used unsteady Navier-Stokes simulations to compute low-Reynolds-number flows over airfoils. Their results show that the separation bubble is unsteady with an associated periodic vortex shedding. The dominant frequency was shown to be in agreement with the most amplified frequency from the linear stability analysis, of a mixing layer corresponding to the separated boundary layer. The instability of the separated flow and the growth of disturbances in the separation bubbles have been previously studied.^[13] Hildings^[14] studied transitional separation bubbles on a flat plate using direct numerical simulations. His results also show that the growth of small disturbances in the separated region

*Graduate Student, Member AIAA.

†Associate Professor, Mechanical and Aerospace Engineering Department, Member AIAA, xiaolin@seas.ucla.edu.

agree with results from linear stability analysis. The influence of disturbances on the mean flow has also been shown.

This paper uses two-dimensional numerical simulations to study unsteady low-Reynolds-number subsonic and transonic flows over the APEX airfoil. The APEX airfoil was designed at NASA Dryden for optimal performance in the transonic low-Reynolds-number regime. The airfoil will be used for high altitude flight tests^[2] to collect data in the low-Reynolds-number regime. The present numerical simulations show the unsteady nature of the flow, with periodic vortex shedding. An analysis of the numerical results shows that there is significant growth of small disturbances in the separation bubble, which leads to the periodic vortex shedding. The dominant frequencies and wavenumbers seen in the numerical simulations are in agreement with the results from linear stability calculations. In the transonic case, the presence of shocks is shown to have significant effects on the unsteady flowfield. The computations are performed using a two-dimensional Navier-Stokes solver. A second order implicit Gauss-Seidel method is used for the calculations. The computer code has been modified, using MPI, to run on parallel processing machines.

GOVERNING EQUATIONS

The mass, momentum and energy conservation equations for compressible flows in two dimensions are as follows:

$$\frac{\partial U}{\partial t} + \frac{\partial F}{\partial x} + \frac{\partial G}{\partial y} = 0 \quad (1)$$

where

$$\mathbf{U} = \begin{bmatrix} \rho \\ \rho u \\ \rho v \\ e \end{bmatrix} \quad (2)$$

$$\mathbf{F} = \begin{bmatrix} \rho u \\ \rho u^2 + p + \sigma_{11} \\ \rho uv + \sigma_{12} \\ u(e + p + \sigma_{11}) + \sigma_{12}v + q_1 \end{bmatrix} \quad (3)$$

$$\mathbf{G} = \begin{bmatrix} \rho v \\ \rho uv + \sigma_{21} \\ \rho v^2 + p + \sigma_{22} \\ v(e + p + \sigma_{22}) + \sigma_{21}u + q_2 \end{bmatrix} \quad (4)$$

where σ_{ij} represents the shear stresses and q_1, q_2 are the heat conduction fluxes. The equation of state is as follows:

$$p = (\gamma - 1) \left[e - \frac{1}{2} \rho (u^2 + v^2) \right] \quad (5)$$

The viscosity coefficient is calculated using the Sutherland's law. The Prandtl number (Pr) is taken to be 0.7, and the ratio specific heats (γ) is taken as 1.4. No slip boundary conditions are imposed on the wall.

NUMERICAL METHOD

In the computations, the equations are transformed from the Cartesian coordinates (x, y, t) into the curvilinear computational coordinates (ξ, η, τ). The computations are performed on a C-grid (for airfoil computations). The grids are generated using an elliptic grid generator. An implicit second order finite volume line Gauss-Seidel iteration method^[15] is used for the computations. The inviscid terms are computed using the flux splitting method and central differencing is used for the viscous terms. The computation involves calculations which are implicit in the η (normal) direction, while the ξ (streamwise) direction terms are computed by a line Gauss-Seidel iteration with alternating sweeps in the backward and forward ξ directions. The computations are first order accurate in time, with the time step being small enough to resolve the time dependence of the solution. The explicit part of the code has been modified using MPI to enable computations using parallel processing machines. The computational domain is partitioned and the computations on each subdomain are performed on different processors.

RESULTS

The numerical simulations are used to study subsonic and transonic low-Reynolds-number flows over the APEX airfoil. The unsteady results are analyzed to show the growth of small disturbances in the separation bubble. The dominant frequencies and wavenumbers calculated from the numerical results are compared with the results from the linear stability analysis.

Validation Cases and Numerical Accuracy

The laminar Navier-Stokes solver is validated by computing the incompressible flat plate boundary layer flow. The results are in good agreement with the Blasius boundary layer solution. Inviscid flow over the NACA 0012 airfoil is calculated, as a validation case, for an angle of attack of 10° and a Mach number of 0.3. The C_p distribution is compared with the numerical results from Salas et al.^[16] in Fig. 2, and is found to be in good agreement.

For time-accurate computations of unsteady flows over airfoils, the time step is chosen small enough to ensure that the solution obtained is independent of the time step. This is verified by doing a time step refinement study and confirming that the solution obtained is the same with the smaller time steps and the original time step size. Figure 3 shows the variation of surface pressure with time, at a point on the upper surface, calculated using three different time step sizes ($\Delta t = 1 \times 10^{-6}$, $\Delta t/2$, and $\Delta t/4$). The figure shows that the solution obtained is independent of the time step, for the chosen time step sizes.

The unsteady Navier-Stokes solver is validated by cal-

culating low-Reynolds-number flow over the Eppler 387 airfoil. The computations are performed for the following flow conditions: $Re_\infty = 1 \times 10^5$, $\alpha = 1^\circ$, and $M_\infty = 0.2$. The 314×114 grid used for the computations is shown in Fig. 4. The numerical solution shows the unsteady nature of the separation bubble, with periodic vortex shedding. These results are similar to the numerical results of Lin and Pauley.^[11] Figure 5 shows the variation of the surface pressure, at a point located near the trailing edge, as a function of time. The presence of a dominant frequency is clearly seen from the figure. The time-averaged surface pressure distribution agrees well with the experimental results as shown in Fig. 6. Figure 7 shows the frequency spectrum of the unsteady solution at various locations on the surface of the airfoil. For the locations in the separation bubble, the dominant frequency is $\omega^* = 0.039$. The frequency is nondimensionalized as $\omega^* = \frac{\omega \delta^*}{U_\infty}$, where $\delta^* = x/(\sqrt{Re_x})$, $Re_x = \frac{\rho_\infty U_\infty x}{\mu_\infty}$. The stability of the separated boundary layer is analyzed using a linear stability analysis. The results show that the dominant frequency seen in the numerical results is within 6.5% of the dominant frequency predicted by linear stability theory.

Subsonic Flow Over the APEX Airfoil

The flow over the APEX airfoil was calculated for the following freestream conditions: $\alpha = 4^\circ$, $M_\infty = 0.5$, and $Re_\infty = 2 \times 10^5$. The calculations have been performed using a 410×75 grid (as shown in Fig. 8) and a 602×150 grid. The calculation using the 602×150 grid was performed using the parallel code over eight processors (grid as shown in Fig. 9).

410 × 75 Grid Calculation

The numerical solution shows that the flowfield is unsteady, with periodic vortex shedding, similar to the Eppler 387 case. Figure 10 shows the variation of surface pressure at a fixed point, after the separation point on the upper surface, with time. The presence of a dominant frequency is clearly evident. The vortex shedding process is visualized in Fig. 14 using flowfield streamline plots in sequence, corresponding to one time period. The presence of a dominant wavenumber can also be clearly seen. The unsteady flow leads to a corresponding variation in the surface C_p distribution as shown through a sequence of plots in Fig. 15. The plots clearly show the presence of a dominant wavenumber.

The growth of disturbance waves in the separation bubble was analyzed using the frequency spectrum of pressure disturbances at various points. Figure 16 shows the frequency spectrum of the pressure disturbance at various locations on the upper surface of the airfoil. The growth of the dominant disturbance wave in the separated region is clearly seen. The figure also shows that there is growth of subharmonic frequencies

Table 1: Comparison of numerical results with the linear stability theory (LST).

	LST	Numerical	% Error
α^*	62.51	57.79	7.5
ω_R^*	31.39	28.08	10.5

and subsequently higher frequencies. In this region non-linear effects will be important and may require three dimensional calculations. The initial growth of disturbances in the separation bubble is expected to agree with linear stability theory. This is verified through a linear stability analysis of the time-averaged separated flow profile. The variation of growth rates and frequencies with the wavenumbers are shown in Fig. 11 and Fig. 12 respectively. The frequency and wavenumber corresponding to the most unstable disturbance wave are compared with the dominant frequency and wavenumber from the numerical results in Table 1. The frequency (ω_R) and wavenumber (α) are nondimensionalized as $\alpha^* = \alpha c$, $\omega_R^* = \omega_R \frac{c}{U_\infty}$. Hence, in the separation bubble the most unstable disturbance wave is accurately captured by the numerical solution. This is further verified by the fine grid results presented in the following subsection.

602 × 150 Grid Calculation

The results of the fine grid (602×150) computations are used to verify that the dominant frequency observed is independent of the grid. Figure 17 shows the vortex shedding process through a sequence of streamline plots corresponding to one time period. The dominant frequency ω_R^* is found to be 28.7, which is within 2% of the coarse grid value. The time-averaged C_l value is found to be 0.84, which is within 8% of the coarse grid value. The time-averaged C_p distribution from both the simulations is compared in Fig. 13. The results show that there is a change in the mean flow in the separated region. Hence, the numerical results show that the mean flowfield is influenced by the disturbance waves present in the flowfield. Similar results have been reported by Hildings^[14] in his study of transitional separation bubbles on a flat plate. As seen in Fig. 16 there is growth of subharmonic waves and of higher frequency waves in the separated region. In this region nonlinear and three dimensional effects may become important.

Transonic Flow Over the APEX airfoil

The unsteady Navier-Stokes solver was also used to compute transonic flow over the APEX airfoil. For this case, the presence of shocks is expected to influence the unsteady separation bubble. The computations have been performed for the following flow con-

ditions: $Re = 200,000$, $\alpha = 4^\circ$, and $M = 0.65$. A 605×150 grid is used for the computations. Figure 18 shows the unsteady vortex shedding observed in this case. The results show that there is considerable variation in the separation location. The presence of the shock creates an adverse pressure gradient which moves the separation location towards the leading edge. This results in the shock disappearing from the flowfield, and a corresponding movement in the separation location towards the trailing edge. Hence, there is considerable movement in the separation location during the vortex shedding process. The later stages of the separation bubble are expected to be influenced by three dimensional and nonlinear effects. Further calculations using finer grids and three dimensional grids will be required to assess these effects.

CONCLUDING REMARKS

Unsteady subsonic and transonic low-Reynolds-number flows over the APEX airfoil have been numerically simulated. Both the studies show the unsteady nature of the separated flow, with periodic vortex shedding. For the subsonic case the vortex shedding seen in the numerical results is found to be due to the instability of the separated boundary layer. The numerical results also show the growth of disturbance waves in the separation bubble. The dominant frequency and wavenumber seen in the numerical simulations is found to be in agreement with the most unstable wavenumber and frequency calculated using linear stability theory. This dominant frequency is found to be independent of the grid. The numerical solutions also show that beyond a certain location in the separation bubble there is generation of subharmonics waves, and subsequently, interaction between the fundamental and subharmonic waves. The fine grid results show that these nonlinear effects influence the mean flowfield. For transonic flows, the presence of shocks is shown to significantly influence the separation bubbles. The numerical results show that there is considerable movement in the separation location, resulting in an unsteady flowfield.

ACKNOWLEDGMENTS

This research was supported by NASA Dryden Flight Research Center under Grant NCC 2-374.

References

- [1] Lissman, P., "Low Reynolds Number Airfoils," *Annual Review of Fluid Mechanics*, 1983, pp. 223-239.
- [2] Murray, J., Moes, T., Norlin, K., Bauer, J., Geenen, R., Moulton, B., and Hoang, S., "Piloted Simulation Study of a Balloon-Assisted Deployment of an Aircraft at High Altitude." NASA-TM 104245, 1992.
- [3] Mueller, T., "Low Reynolds Number Vehicles." AGARD-AG 288, 1985.
- [4] Mueller, T. and Batill, S., "Experimental Studies of Separation on Two-Dimensional Airfoils at Low Reynolds Numbers," *AIAA Journal*, Vol. 20(4), 1982, pp. 457-463.
- [5] Leblanc, P., Blackwelder, R., and Liebeck, R., "A Comparison between Boundary Layer Measurements in a Laminar Separation Bubble Flow and Linear Stability Theory Calculations," *Low Reynolds Number Aerodynamics: Proceedings of the Conference*, Notre Dame, IN., June 5-7, 1989. Springer-Verlag, 1989.
- [6] Dovgal, A. V., Kozlov, V. V., and Michalke, A., "Laminar Boundary Layer Separation: Instability and Associated Phenomena," *Progress of Aerospace Sciences*, Vol. 30, 1994, pp. 61-94.
- [7] McGhee, R., Walker, B., and Millard, B., "Experimental Results for the Eppler387 Airfoil at Low Reynolds Numbers in the Langley Low-Turbulence Pressure Tunnel," NASA TM4062, 1988.
- [8] Drela, M. and Giles, M., "Viscous-Inviscid Analysis of Transonic and Low Reynolds Number Airfoils," *AIAA Journal*, Vol. 25, 1987, pp. 1347-1355.
- [9] Schneider, J. and Ewald, B., "Integration of Linear Stability Methods into Navier-Stokes Solvers for Computation of Transonic Laminar Airfoils," AIAA Paper 94-1849-CP, 1994.
- [10] Vatsa, V. and Carter, J., "Analysis of Airfoil Leading-Edge Separation Bubbles," *AIAA Journal*, Vol. 22(12), 1984, pp. 1697-1704.
- [11] Lin, J. M. and Pauley, L. L., "Low-Reynolds-Number Separation on an Airfoil," *AIAA Journal*, Vol. 34(8), 1996, pp. 1570-1577.
- [12] Drela, M., "Transonic Low-Reynolds-Number Airfoils," *Journal of Aircraft*, Vol. 29(6), 1992, pp. 1106-1113.
- [13] Tatini, M. and Zhong, X., "Numerical Simulation of Unsteady Low-Reynolds-Number Separated Flows Over Airfoils," AIAA Paper 97-1929, 1997.
- [14] Hildings, C., "Simulation of Laminar and Transitional Separation Bubbles," *Technical Reports from Royal Institute of Technology, Sweden*, Technical Report 1997:19, 1997.
- [15] MacCormack, R., "Current Status of Numerical Solution of the Navier Stokes Equations." AIAA Paper 85-0032, 1985.

- [16] Salas, M. D., Jameson, A., and Melnik, R. E., "A Comparative Study of the Non-uniqueness Problem of the Potential Equation," AIAA Paper 83-1888, 1983.
- [17] King, L. S., "A Comparison of Turbulence Closure Models for Transonic Flows About Airfoils," AIAA Paper 87-0418, 1987.
- [18] Yang, Z. and Voke, P. R., "Numerical Study of Mechanisms of Boundary Layer Transition After a Separation Bubble," *Advances in Turbulence VI*, Kluwer Academic Publishers, 1996, pp. 55-58.

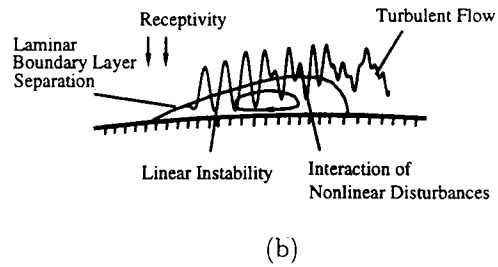
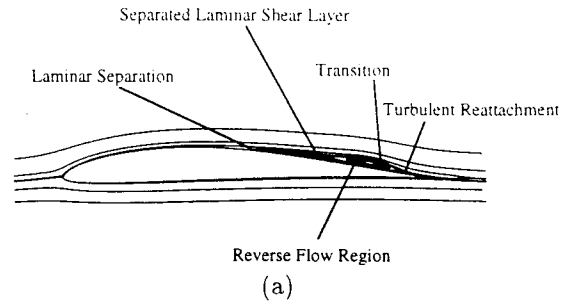


Figure 1: (a) Structure of the separation bubble for low-Reynolds-number flows, (b) a schematic detailing the growth of disturbances in various regions of the separation bubble.

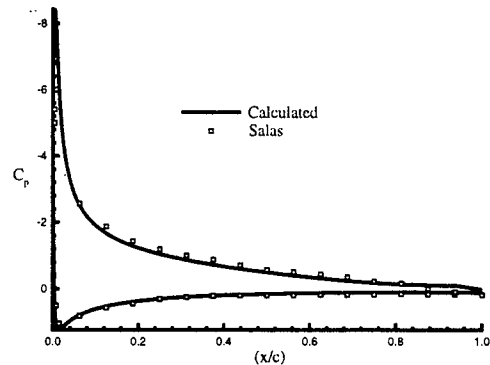


Figure 2: Comparison of the calculated C_p distribution with the numerical results from [16]. Flow over the NACA 0012 airfoil at $\alpha = 10^\circ$ and $M = 0.3$.

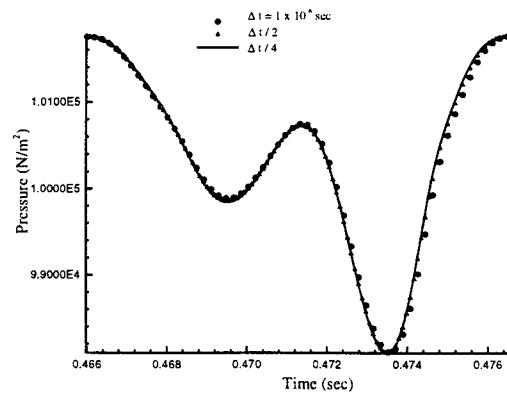


Figure 3: Variation of surface pressure with time, at a point on the upper surface, calculated using three different time step sizes to verify the time accuracy. Flow over the Eppler 387 airfoil at $M_\infty = 0.2$, $Re_\infty = 1 \times 10^5$, and $\alpha = 1^\circ$.

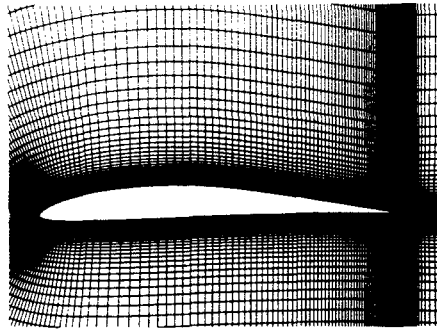


Figure 4: A section of the 314×114 grid used for the computations over the Eppler 387 airfoil.

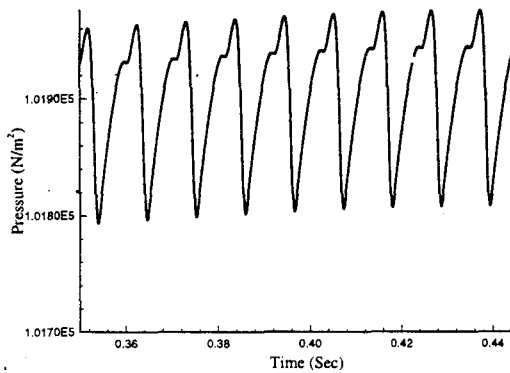


Figure 5: The variation of surface pressure at a fixed point, near the trailing edge, with time. Flow over the Eppler 387 airfoil at $M_\infty = 0.2$, $Re_\infty = 1 \times 10^5$, and $\alpha = 1^\circ$.

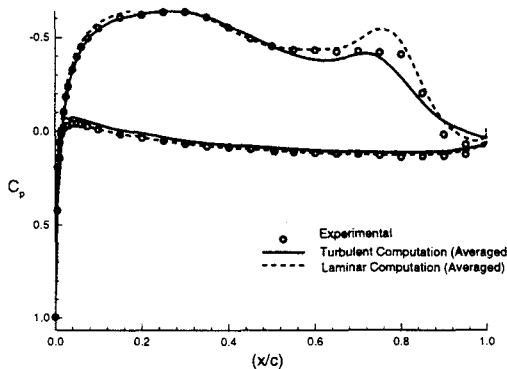


Figure 6: Time averaged C_p distributions for the laminar and turbulent solutions compared with experimental results. Flow over the Eppler 387 airfoil at $M_\infty = 0.2$, $Re_\infty = 1 \times 10^5$, and $\alpha = 1^\circ$.

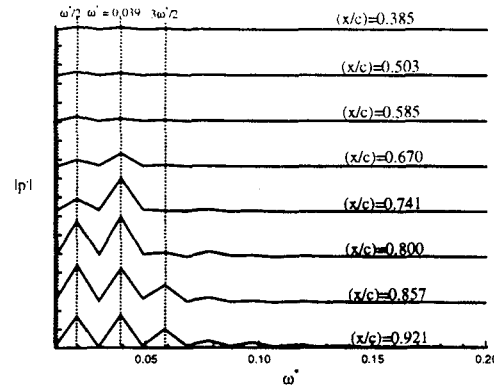


Figure 7: Frequency spectrum of the pressure disturbance at various locations on the upper surface of the airfoil. Flow over the Eppler 387 airfoil at $M_\infty = 0.2$, $Re_\infty = 1 \times 10^5$, and $\alpha = 1^\circ$.

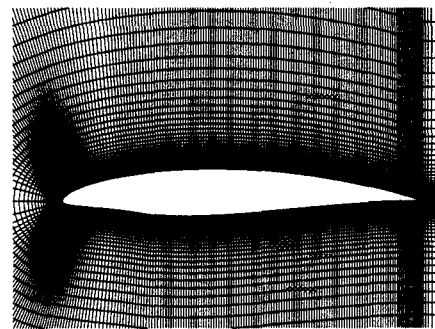


Figure 8: A section of the 410×75 grid used for the computations over the APEX airfoil. $M_\infty = 0.5$, $Re_\infty = 2 \times 10^5$, and $\alpha = 4^\circ$.

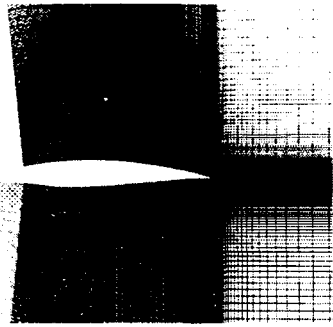


Figure 9: A section of the 602×150 grid used for the computations over the APEX airfoil (distributed over 8 processors). $M_\infty = 0.5$, $Re_\infty = 2 \times 10^5$, and $\alpha = 4^\circ$.

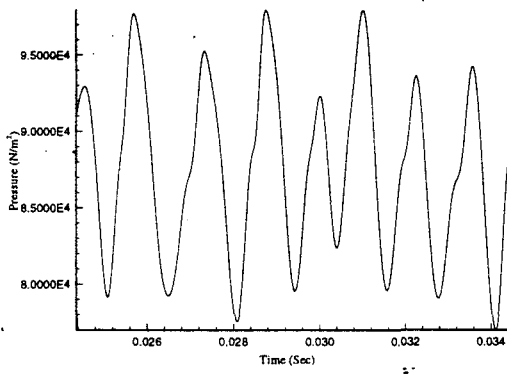


Figure 10: The variation of surface pressure at a fixed point, after the separation point on the upper surface, with time. Flow over the APEX airfoil at $M_\infty = 0.5$, $Re_\infty = 2 \times 10^5$, and $\alpha = 4^\circ$.

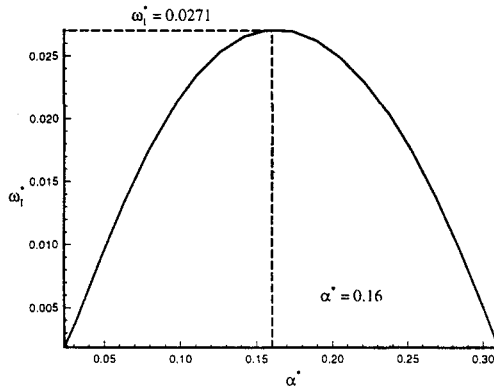


Figure 11: The variation of the growth rates with wavenumbers. Results obtained from the linear stability analysis ($\alpha^* = \alpha \delta^*$ and $\omega_i^* = \omega_i \frac{\delta^*}{U_\infty}$). Flow over the APEX airfoil at $M_\infty = 0.5$, $Re_\infty = 2 \times 10^5$, and $\alpha = 4^\circ$.

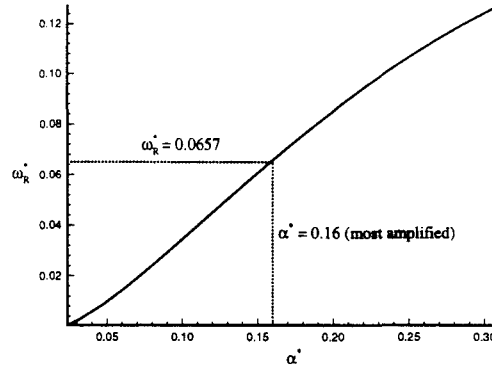


Figure 12: The variation of the frequency with wavenumbers. Results obtained from the linear stability analysis ($\alpha^* = \alpha \delta^*$ and $\omega_r^* = \omega_r \frac{\delta^*}{U_\infty}$). Flow over the APEX airfoil at $M_\infty = 0.5$, $Re_\infty = 2 \times 10^5$, and $\alpha = 4^\circ$.

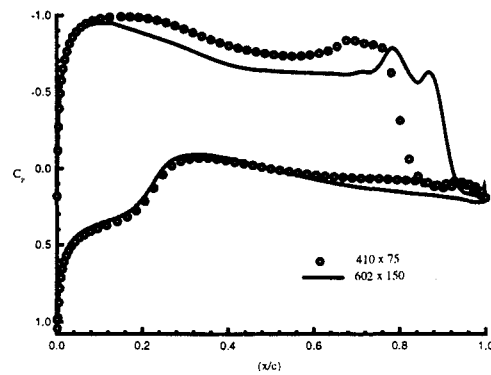


Figure 13: Comparison of the time-averaged C_p distribution from the coarse and fine grids. Flow over the APEX airfoil at $M_\infty = 0.5$, $Re_\infty = 2 \times 10^5$, and $\alpha = 4^\circ$.

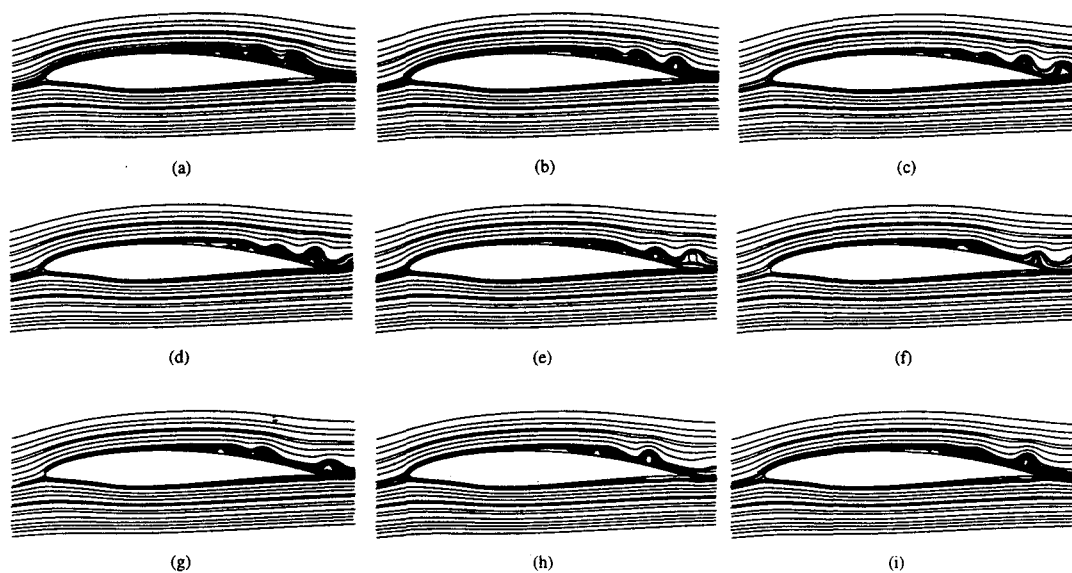


Figure 14: Flowfield streamline plots (a)-(i) in sequence, corresponding to one time period, showing the vortex shedding process. The corresponding pressure distribution is shown by color contour levels. Flow over the APEX airfoil at $M_\infty = 0.5$, $Re_\infty = 2 \times 10^5$, and $\alpha = 4^\circ$. Computations using a 410×75 grid.

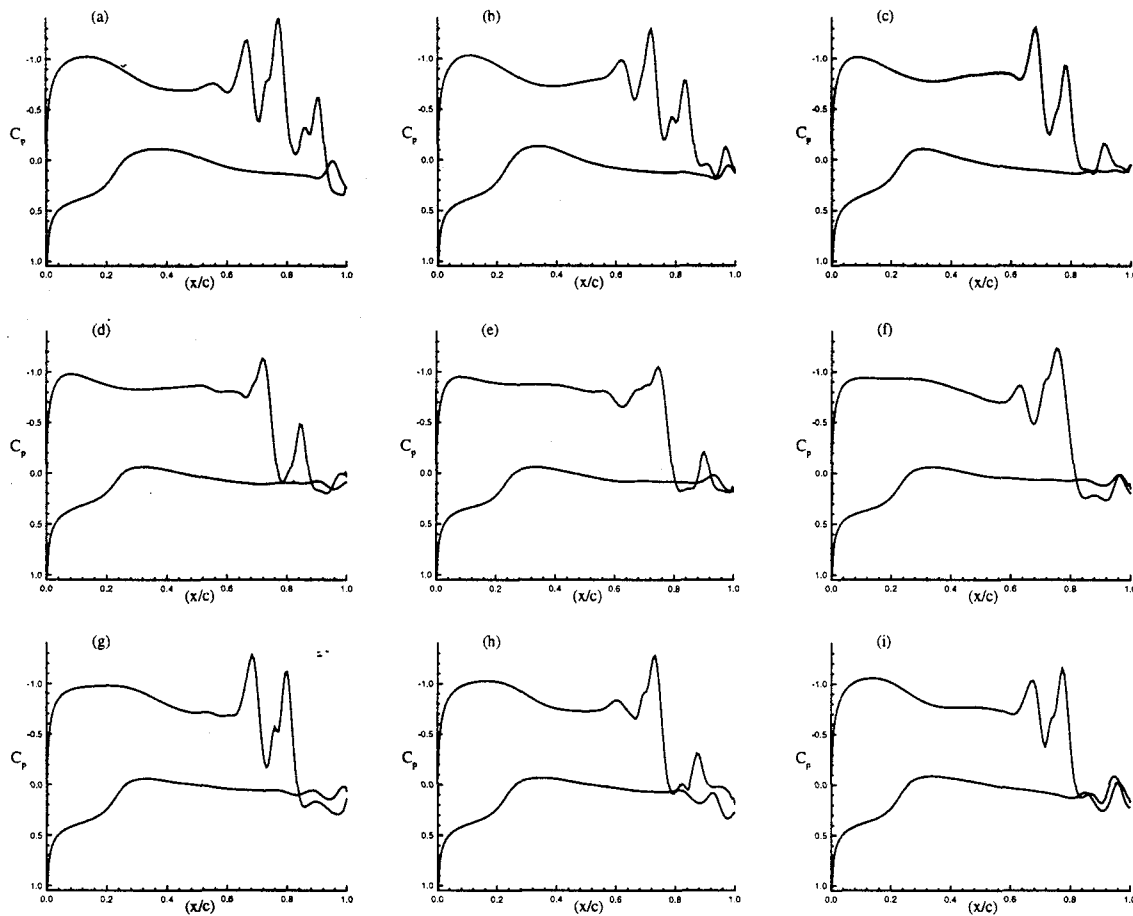


Figure 15: Variation of C_p with time, (a)-(i) in sequence, corresponding to one time period. Flow over the APEX airfoil at $M_\infty = 0.5$, $Re_\infty = 2 \times 10^5$, and $\alpha = 4^\circ$ Computations using a 410×75 grid.

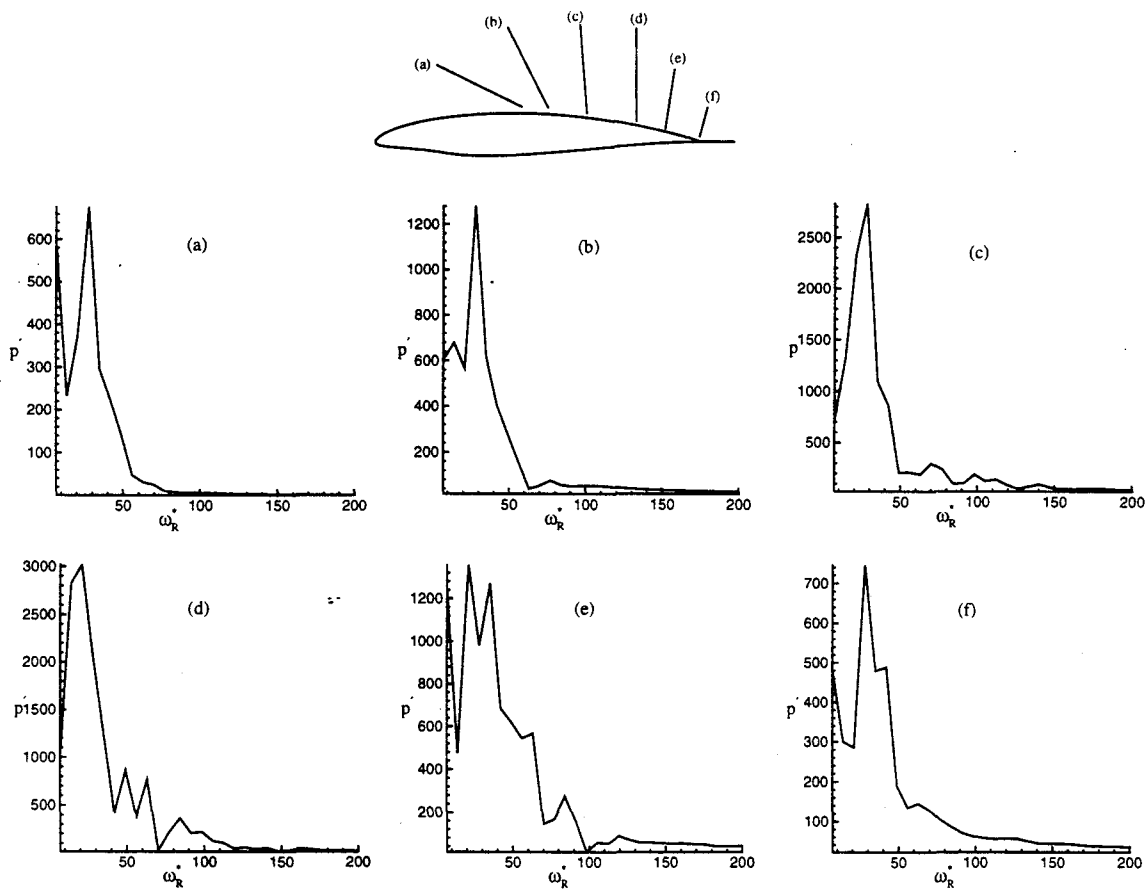


Figure 16: Frequency spectrum of the pressure disturbance at various locations on the upper surface of the airfoil. Flow over the APEX airfoil at $M=0.5$, $Re = 2 \times 10^5$, $\alpha = 4^\circ$.

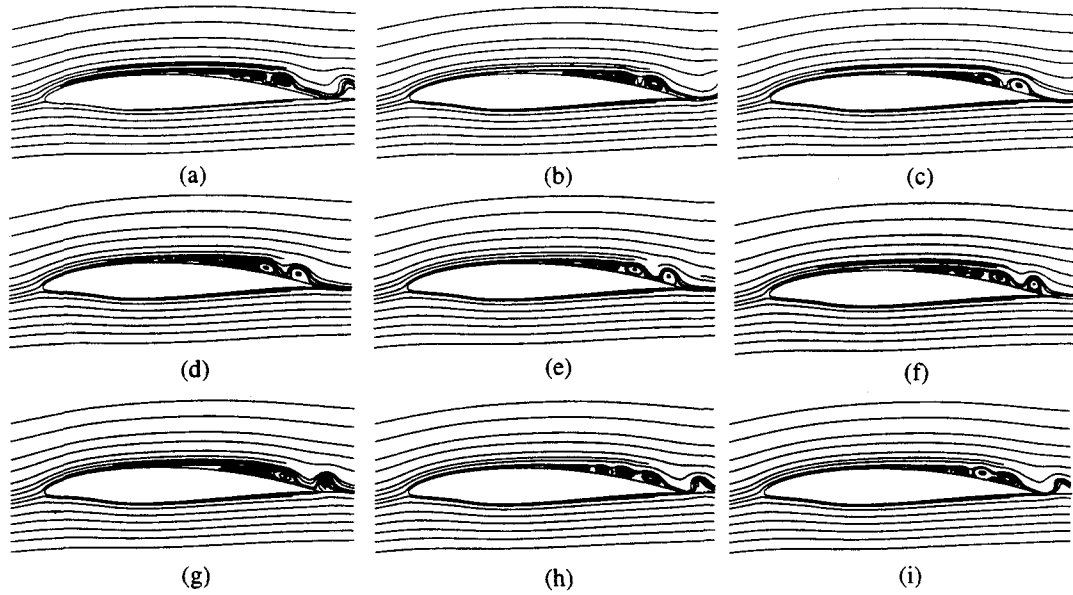


Figure 17: Vortex shedding process visualization using a sequence of streamline plots, corresponding to one time period. Flow over the APEX airfoil at $M_\infty = 0.5$, $Re_\infty = 2 \times 10^5$, and $\alpha = 4^\circ$. Computations using a 602×150 grid.

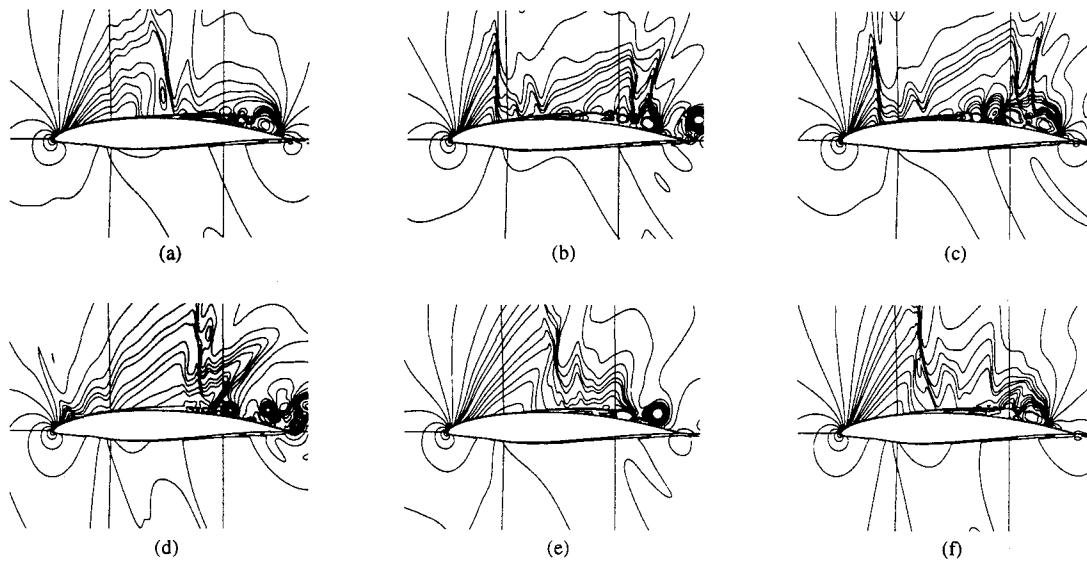


Figure 18: Visualization of the vortex shedding process using flowfield pressure contours, (a)-(f) in sequence, corresponding to one time period. Flow over the APEX airfoil at $M_\infty = 0.65$, $Re_\infty = 2 \times 10^5$, and $\alpha = 4^\circ$.